Thermochromic VO[2] nanorods made by sputter deposition: Growth conditions and optical modeling

AUTHOR(S):

Li, Shu-Yi; Namura, Kyoko; Suzuki, Motofumi; Niklasson, Gunnar A.; Granqvist, Claes G.

CITATION:

Li, Shu-Yi ...[et al]. Thermochromic VO[2] nanorods made by sputter deposition: Growth conditions and optical modeling. Journal of Applied Physics 2013, 114(3): 033516.

ISSUE DATE:

2013

URL:

http://hdl.handle.net/2433/192291

AIP | Journal of Applied Physics

Thermochromic VO2 nanorods made by sputter deposition: Growth conditions and optical modeling

Shu-Yi Li, Kyoko Namura, Motofumi Suzuki, Gunnar A. Niklasson, and Claes G. Granqvist

Citation: Journal of Applied Physics **114**, 033516 (2013); doi: 10.1063/1.4813876
View online: http://dx.doi.org/10.1063/1.4813876
View Table of Contents: http://scitation.aip.org/content/aip/journal/jap/114/3?ver=pdfcov
Published by the AIP Publishing

JOURNAL OF APPLIED PHYSICS **114**, 033516 (2013)

Thermochromic VO_2 nanorods made by sputter deposition: Growth conditions and optical modeling

Shu-Yi Li,[1,a)] Kyoko Namura,[2,b)] Motofumi Suzuki,[2] Gunnar A. Niklasson,[1] and Claes G. Granqvist[1]
[1]*Department of Engineering Sciences, The Ångström Laboratory, Uppsala University, P.O. Box 534, SE-75121 Uppsala, Sweden*
[2]*Department of Micro Engineering, Kyoto University–Katsura, C3 b4N01, Kyoto 615–8540, Japan*

(Received 30 May 2013; accepted 26 June 2013; published online 17 July 2013)

Reactive dc magnetron sputtering onto glass-based substrates yielded deposits of thermochromic VO_2 with well-developed nanorods and nanowires. Their formation was promoted by high substrate temperature (above ~500 °C), sufficient film thickness, proper inlet of the reactive gas, dispersed gold "seeds," and pronounced substrate roughness. Rutherford back scattering ascertained mass thicknesses, scanning electron microscopy depicted the nanostructures, and glancing incidence X-ray diffraction proved that single-phase VO_2 was normally formed. Spectrophotometric measurements of total and diffuse transmittance and reflectance on VO_2 thin films, at room temperature and ~100 °C, allowed us to determine complex dielectric functions below and above the "critical" temperature for thermochromic switching (~68 °C). These data were then used in computations based on the Bruggeman effective medium theory applied to randomly oriented prolate spheroidal structural units to derive the optical properties of the deposits. Experimental and computed data on spectral absorptance were found to be in good qualitative agreement. © *2013 AIP Publishing LLC*. [http://dx.doi.org/10.1063/1.4813876]

I. INTRODUCTION

This paper presents a comprehensive study on thermochromic VO_2 nanorods and nanowires prepared by sputter deposition and discusses the critical nature of their growth conditions as well as modeling of their optical properties by effective medium theory.

Vanadium dioxide undergoes a reversible metal–insulator transition at a "critical" temperature τ_c of 68 °C.[1] The low-temperature phase is monoclinic, semiconducting, and infrared transparent, while the high-temperature phase is tetragonal, metallic, and infrared-reflecting. The exact nature of the metal–insulator transition has remained elusive and is of continuing scientific interest; recent work has emphasized the significance of electron–electron interactions associated with a Mott–Hubbard transition and/or electron–phonon interactions associated with a Peierls mechanism.[2–9] The value of τ_c can be changed by substitutional doping, for example by replacing some vanadium by tungsten,[10] and well-crystallized $W_xV_{1-x}O_2$ films with $x \approx 0.02$ can have $\tau_c \approx 20$ °C;[11] doping with atomic hydrogen is another possibility.[12] The magnitude of the resistance change at τ_c depends on the degree of crystallinity, and epitaxial films can display a difference of three to four orders of magnitude.[13] The luminous transmittance can be boosted by magnesium substitution[14,15] and by fluorination.[16]

The metal–insulator transition can be influenced by a variety of external parameters, and recent work has considered the effects of strain[17–19] and lattice misfit with the substrate,[20,21] electric field or current activation,[22–31] light irradiation,[32–38] ion bombardment,[39,40] and gaseous ambience.[41] Considering the wealth of possibilities to modulate the properties of VO_2-based thin films, it is not surprising that they are discussed for a vast number of applications such as thermochromic "smart" windows for energy efficient buildings,[42–50] variable-thermal-emittance surfaces for thermal radiation control,[51] oscillators and switches in (opto)electronics,[25,26,34,52,53] transistors of different types,[30,54,55] microcantilevers,[56,57] memory elements,[58] infrared imaging devices[36] and spatial modulators for electromagnetic radiation,[37,59] (micro)bolometers,[60–63] and sensors for humidity[64] and gas.[41]

It was recently realized that nanothermochromism—involving VO_2-based nanoparticles—can entail optical properties of primary interest for energy efficient fenestration.[11,65–67] Consequently, it is of great importance to develop efficient methods to prepare such nanoparticles in large quantities and over extended surfaces. In fact, there have been numerous prior studies on VO_2-based nanoparticles, and recent investigations have been conducted with hydrothermal/solvothermal/colloidal techniques,[27,49,50,64,68–108] vapor transport,[56,109–115] anodization,[116] polymer-assisted deposition,[117,118] and templating.[29,119] References to earlier studies on the manufacturing of nanostructured VO_2-based materials can be found elsewhere.[65,66]

Most of the work reported so far has dealt with materials preparations requiring long times for sample growth and/or post treatment or being suitable for small batches and small surfaces. However, it was recently demonstrated by Cheng *et al.*[120] that "simple" thermal evaporation could yield high-quality VO_2 nanowires on roughened quartz substrates preferably heated to temperatures between 800 and 850 °C. In

a)Author to whom correspondence should be addressed. Electronic mail: Shuyi.Li@angstrom.uu.se.
b)Japan Society for the Promotion of Science (JSPS) Research Fellow.

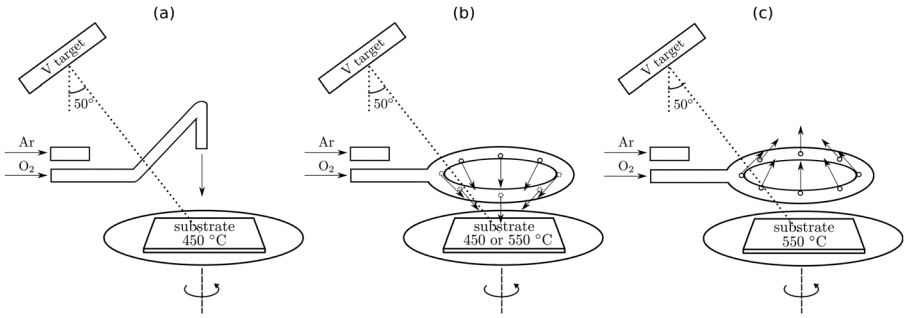

FIG. 1. Target–substrate geometry and provisions for gas inlet into the sputter chamber.

the present work, we employ another physical vapor deposition technique, viz., reactive dc magnetron sputtering and demonstrate that VO_2 nanowires can be grown onto coated or uncoated glass surfaces at temperatures of around 500 °C. It should be noted that magnetron sputtering is an extremely well established industrial technique for cost-efficient large-area deposition onto rigid and flexible substrates.[121,122]

II. SAMPLE PREPARATION

Nanorods and thin films of VO_2 were prepared by reactive dc magnetron sputtering in a versatile deposition system based on a Balzers UTT 400 unit. The deposition chamber was evacuated to 6.3×10^{-7} mbar, and 80 ml/min of argon and 5 ml/min of oxygen (both 99.997%) were then introduced through mass-flow-controlled regulators; the total pressure was maintained at 1.2×10^{-2} mbar. Sputtering took place from a 5-cm-diameter target of vanadium (99.5%) at a power of 172 W. The substrates were of three kinds: (i) 1-mm-thick glass slides (Thermo Scientific), (ii) such glass coated with 4.2-nm-thick gold films sputter-deposited at room temperature, and (iii) glass coated with ~50-nm-diameter silica "nanopillars" prepared by glancing angle deposition and having gold "caps," as reported elsewhere[123] (cf. Fig. 5 below). The latter substrate was included since large surface roughness is known[120] to have a beneficial influence on VO_2 growth. The gold films were non-uniform, as expected from their small mass thickness.[124–127] The substrates were maintained at 450 ± 10 or 550 ± 10 °C during the depositions, as estimated from thermocouple-based recordings, and were rotated at 30 to 60 rpm. The substrate–target separation was 13 cm, and the angle between the normals to the substrate and target was 50°. The O_2 inlet was found to be important for the samples, and we used three arrangements as illustrated in Fig. 1: (a) a simple downwards-pointing tube located centrally above the substrate, (b) a perforated toroidal gas inlet with holes obliquely facing the substrate, and (c) the same gas inlet with the holes obliquely directed away from the substrate.

In all, we prepared more than 30 samples under a large variety of deposition conditions and selected 11 of them for closer examination. Their preparation characteristics are summarized in Table I, where the second, third, fourth, and fifth columns indicate specific gas inlet arrangement (cf. Fig. 1), substrate temperature τ_s during deposition, substrate type, and mass thickness, respectively. The final column indicates the prevailing film morphology, as illustrated and discussed below.

III. STRUCTURE AND COMPOSITION

A. Rutherford backscattering spectrometry

Samples 1, 2, 7, and 9 were investigated by Rutherford backscattering spectrometry (RBS) at the Uppsala Tandem Laboratory, employing 2 MeV ^{4}He ions backscattered at an angle of 170°. Figure 2 shows measured RBS spectra as well as data fitted to a model of the deposit–substrate system by use of the SIMNRA program.[128]

RBS data yield the stoichiometry and the number of atoms per area unit, which combined with thickness measurements (see below) can be used to determine the density of the sputter deposited films. The compact VO_2 film, referred to as sample 1, had 550×10^{15} atoms/cm^2 and its observed

TABLE I. Fabrication parameters and morphology of VO_2 samples. Gas inlets (a)–(c) refer to Fig. 1. Samples indicated by bold sample numbers were subjected to detailed analysis, including optical modeling.

Sample No.	Gas inlet	Temperature (°C)	Substrate	Mass thickness (nm)	Morphology
1	a	450	Glass	62.5	Compact film Fig. 3(a)
2	b	450	Glass	62.5	Rough film with grains Fig. 3(b)
3	b	550	Glass	34	Small elongated grains Fig. 3(c)
4	b	550	Au/glass	34	Short rods Fig. 3(d)
5	b	550	Glass	68	Large elongated grains Fig. 3(e)
6	b	550	Au/glass	68	Moderate rods Fig. 3(f)
7	c	550	Glass	68	Short rods Fig. 4(a)–4(c)
8	c	550	Au/glass	68	Occasional long rods Figs. 4(d)–4(f)
9	c	550	Glass	102	Dense long rods Figs. 4(g)–4(i)
10	c	550	Au/glass	102	Long rods and long wires Figs. 4(j)–4(l)
11	a	450	Au/SiO_2 nanopillars/glass	34	Long wires Fig. 5

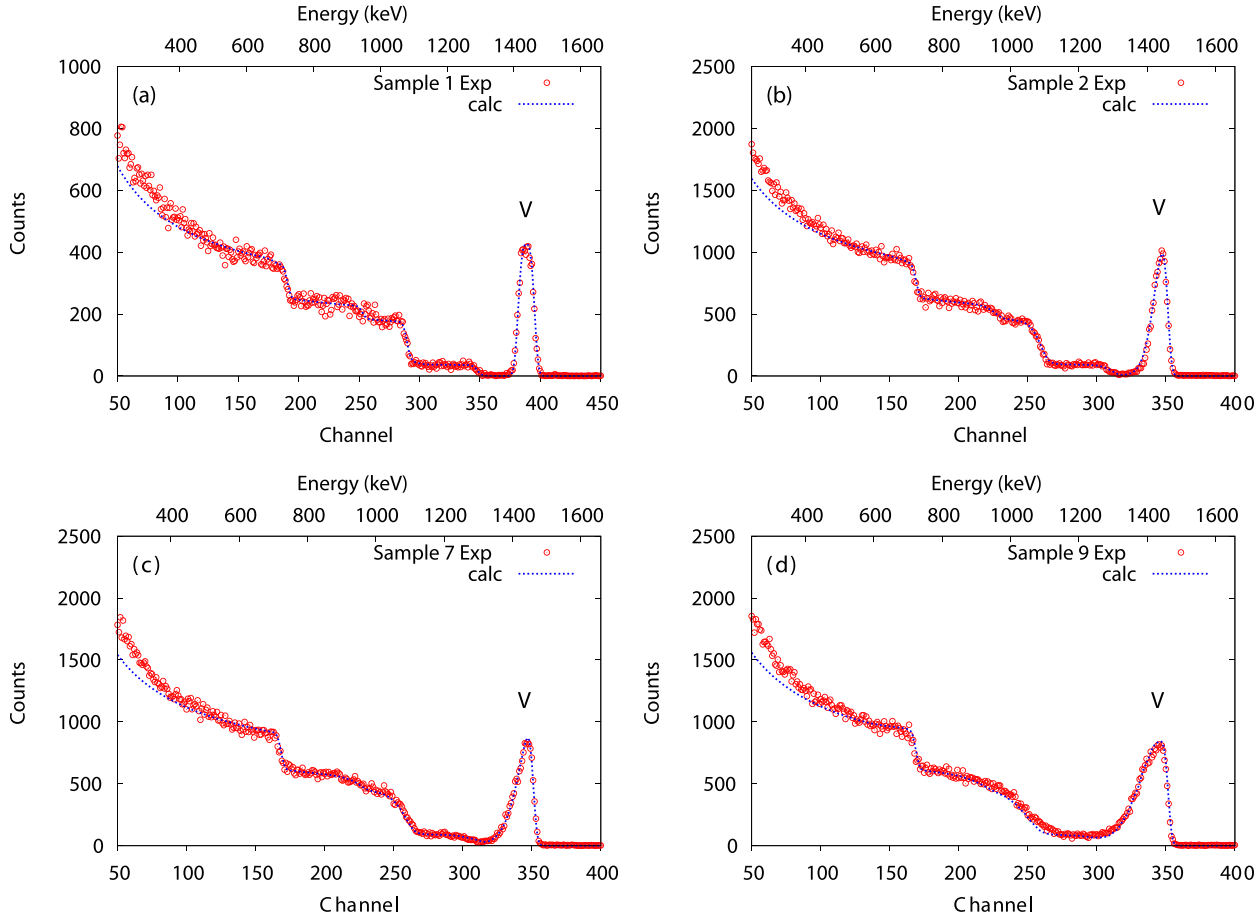

FIG. 2. Experimental (circles) and simulated (dotted curves) RBS data for four VO_2 samples grown under the conditions stated in Table I.

thickness was 62.5 nm, which gives a density of 4.04×10^3 kg/m^3. This is about 11% smaller than the density 4.571×10^3 kg/m^3 for bulk crystalline monoclinic VO_2; a reduced density is expected in sputter-deposited films as a consequence of structural imperfections such as grain boundaries, vacancies, and incorporated gas molecules. Mass thicknesses d for samples 2, 7, and 9 were determined from RBS data, assuming the same density as in sample 1, and mass thicknesses for the remaining samples were inferred from scaling with deposition time. These thicknesses are reported in Table I and are judged to be accurate to $\pm 5\%$.

The analysis using the SIMNRA program allows assessment of sample inhomogeneity, and the asymmetrical vanadium peak exhibited by samples 2, 7, and 9 (Figs. 2(b)–2(d))—especially for samples 7 and 9—gave evidence for strong fluctuations in the area density of vanadium atoms, as expected for deposits comprised of nanorods and nanowires. Sample 1, on the other hand, displayed a symmetrical vanadium peak (Fig. 2(a)), which signals homogeneity.

B. Scanning electron microscopy

All of the samples listed in Table I were studied by scanning electron microscopy (SEM), specifically using a LEO 1550 FEG Gemini instrument with an acceleration voltage of 10 to 15 kV. Imaging was done in three ways: (i) with the electron beam perpendicular to the sample surface, (ii) with the sample's surface normal tilted 70° off the beam direction, and (iii) for the cross-section of a fractured sample. The latter measurements yield a "geometrical" sample thickness, which exceeds d for samples with pronounced nanofeatures.

Figure 3 shows SEM micrographs for samples 1–6, which were prepared with downward-directed gas flow. Panels (a) and (b) refer to samples 1 and 2, which were deposited with approximately the same values of $\tau_s \approx 450$ °C and $d \approx 62.5$ nm, on identical glass substrates, but with different arrangements for the gas inlet. The average grain sizes of the VO_2 deposits differ significantly and were ~28 nm for the tube inlet (Fig. 1(a)) and ~45 nm for the toroidal inlet (Fig. 1(b)), implying that the morphology is critically dependent on the detailed deposition conditions. Samples 3 and 4, reported on in Figs. 3(c) and 3(d), have similar magnitudes of $\tau_s \approx 550$ °C and $d \approx 34$ nm, employed the same type of gas inlet (Fig. 1(b)), but were grown on different types of substrates; sample 3 was deposited onto bare glass and sample 4 onto gold-seeded glass. Again the sample morphologies are markedly different, and the deposit on glass showed elongated grains with maximum lengths of ~200 nm, whereas the deposit on gold displayed grains with lengths up to ~500 nm. There is also a clear dependence on the deposit thickness, as found for samples 5 and 6 depicted in Figs. 3(e) and 3(f). These samples have $d \approx 68$ nm, i.e., they are twice as thick as samples 3 and 4 but were otherwise identical with regard to deposition parameters. The most noteworthy

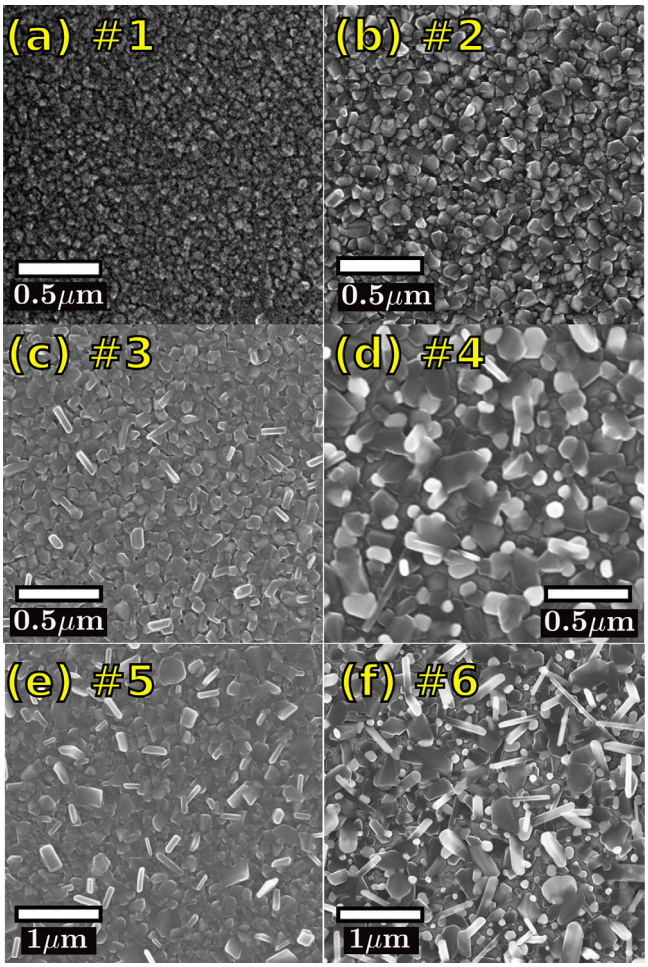

FIG. 3. Scanning electron micrographs (top views) for VO_2 samples 1–6 grown under the conditions stated in Table I. Note that the magnification of samples 1–4 is different from that of samples 5 and 6.

difference is between Figs. 3(d) and 3(f), referring to deposits on gold-seeded glass, and demonstrates that the deposit attains a decidedly rod-like character at $d \approx 68$ nm whereas rods are much less prevalent at $d \approx 34$ nm. A close inspection of Fig. 3(d) shows that many of the rods have "caps" of gold, which suggests that VO_2 has grown from underneath the gold seeds. The substrate temperature is another important factor, and a comparison of Fig. 3(b) obtained at $\tau_s \approx 450\,^{\circ}C$ with Figs. 3(c) and 3(e) obtained at $\tau_s \approx 550\,^{\circ}C$ shows that high substrate temperature facilitates a structure comprising elongated grains. Summarizing some of the main results in Fig. 3, one finds that the growth of VO_2 nanorods is promoted by high substrate temperature, large deposit thickness, and gold seeding.

Figure 4 depicts SEM images recorded on samples 7–10 prepared at $\tau_s \approx 550\,^{\circ}C$ with obliquely upwards-directed gas flow (Fig. 1(c)). The first column of micrographs was taken with the electron beam perpendicular to the sample surface, the middle column with the sample's surface normal tilted 70° off the beam direction, whereas the right-hand column shows cross-sections of fractured samples. The first and third rows of images refer to depositions onto bare glass and the second and fourth (bottom) rows refer to gold-seeded glass. Comparing the SEM micrographs in Fig. 4 for deposits on bare and gold-seeded glass, it is again apparent that gold promotes the formation of well-developed VO_2 nanorods and nanowires. In particular, it is noteworthy that nanorods exceeding 5 μm in length could be produced with considerable density for $\tau_s \approx 550\,^{\circ}C$ and $d \approx 102$ nm, as apparent from Fig. 4(j). Furthermore, it is interesting to compare data for samples 7 and 8 (Figs. 4(a), 4(b), 4(d), and 4(e)) with data for samples 5 and 6 (Figs. 3(e) and 3(f)); the former samples were prepared with a toroidal gas inlet with perforation directed obliquely away from the substrate (Fig. 1(c)), while the latter samples used the same gas inlet though with perforation obliquely facing the substrate (Fig. 1(b)), while all of the samples were made with the same values of $\tau_s \approx 550\,^{\circ}C$ and $d \approx 68$ nm. This comparison demonstrates once again that details of the gas inlet play a pervasive role for the nanostructure of the deposits, and it is evident that nanorods and nanowires are better developed when the oxygen is directed obliquely away from the substrate. The cross-sectional SEM micrographs in Figs. 4(c), 4(f), 4(i), and 4(l) give striking evidence for nanorod and nanowire formation and also indicate that the deposits exhibit a two-layer structure with a highly porous top layer and a much more compact bottom layer.

Figure 5 shows cross-sectional views of sample 11 for which sputter deposition took place onto a substrate with silica "nanopillars" having gold "caps" as indicated in panel (c). The simple gas inlet in Fig. 1(a) was used, together with $\tau_s \approx 450\,^{\circ}C$. Despite the small mass thickness $d \approx 34$ nm, the deposit has developed nanowires more than two micrometers in length, which reiterates the large importance of the substrate conditions.

C. X-ray diffractometry

Grazing incidence X-ray diffraction (GIXRD) measurements were done for diffraction angles in the $10 < 2\theta < 80°$ range and at room temperature by use of a Siemens D5000 Th-2Th instrument. Data are shown in Fig. 6 for samples 1, 2, 7, and 9; the diffractograms are found to agree well with the standard pattern for monoclinic VO_2 with space group $P21/c$.[129] Rietveld refinement[130] was performed on the GIXRD spectra using the PowderCell 2.3 program[131] and suggested that samples 7 and 9 are consistent with the March–Dollase model[132] and exhibit moderate preferential growth in the (100) direction. Sample 9 displayed some additional tiny diffraction peaks for 2θ. Those at 12.2°, 25.88°, and 34.4° may tentatively be associated with V_2O_5 (Refs. 133 and 134) or V_2O.[135]

IV. OPTICAL PROPERTIES

A. Measured data and evaluated complex dielectric function

Spectral total transmittance $T(\lambda)$ and reflectance $R(\lambda)$, as well as spectral diffuse transmittance $T_d(\lambda)$ and reflectance $R_d(\lambda)$, were measured in the $300 < \lambda < 2500$ nm wavelength interval by use of a Perkin–Elmer Lambda 900 double-beam spectrophotometer equipped with a $BaSO_4$-coated integrating sphere. Data were recorded for normal incidence at room temperature and at 100 °C, where the latter temperature is

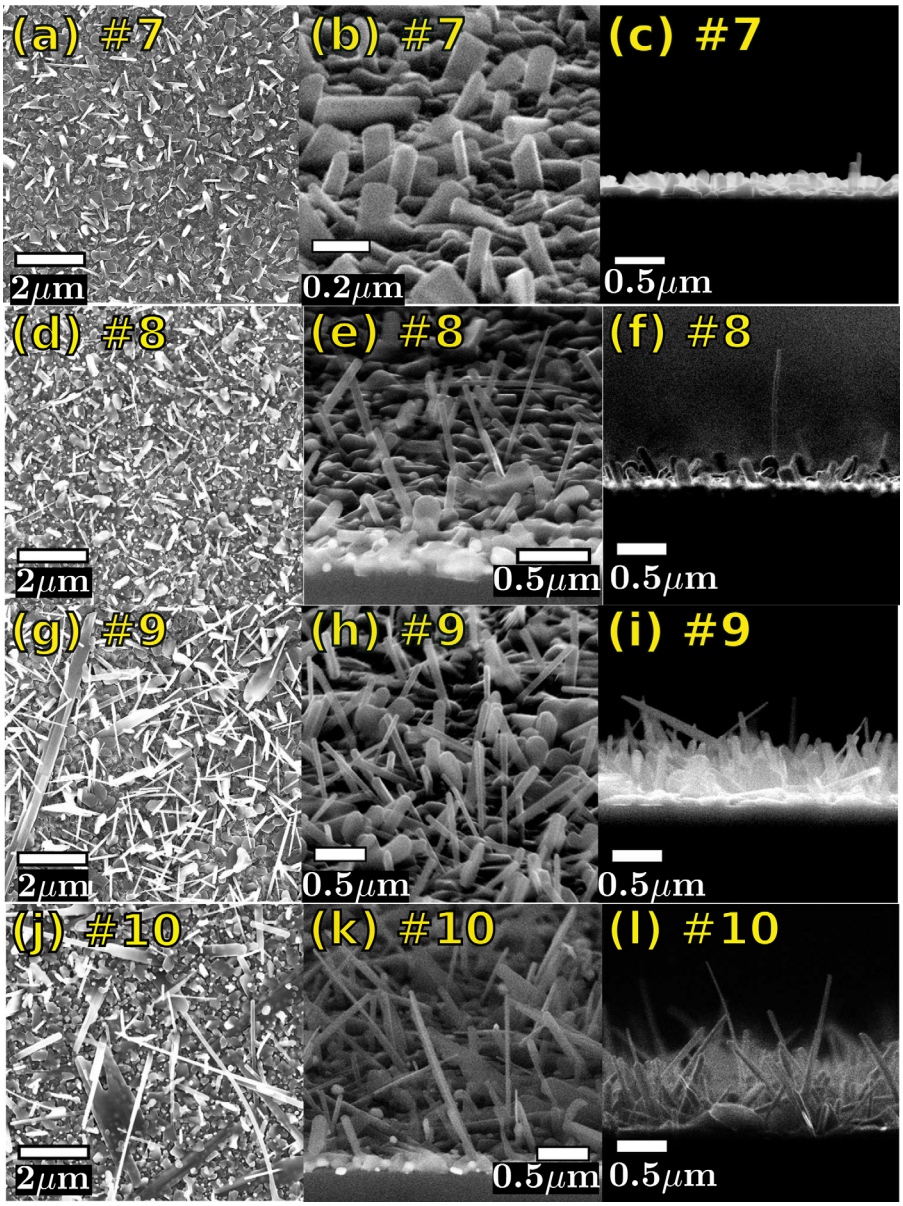

FIG. 4. Scanning electron micrographs for VO_2 samples 7–10 grown under the conditions stated in Table I. Left-hand, middle, and right-hand columns refer to top views, imaging at 70° between electron beam and sample normal, and cross-sectional views, respectively. Note that the magnifications differ among the various images.

well above τ_c. The diffuse components represent light that was not specularly reflected or transmitted through the sample, as elaborated elsewhere.[136] Our reflectance standard was a plate coated with $BaSO_4$.

Figure 7 shows $T(\lambda)$ and $R(\lambda)$ for samples 1, 2, 7, and 9. The former three of these have roughly the same mass thickness, whereas sample 9 is thicker. Thermochromism is evident, as expected, and the infrared transmittance is

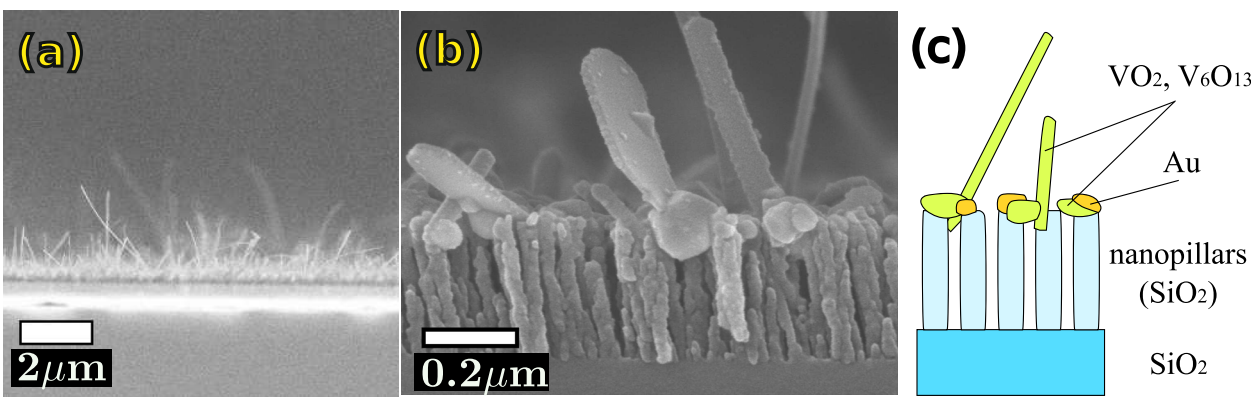

FIG. 5. Panels (a) and (b) show scanning electron micrographs (cross-sectional views) for VO_2 sample 11, grown under the conditions stated in Table I, and provides an overview image as well as a magnification of the substrate and the lower part of some of the nanowires, respectively. Note that the magnifications are different for these two images. Panel (c) is a schematic rendition of the investigated sample.

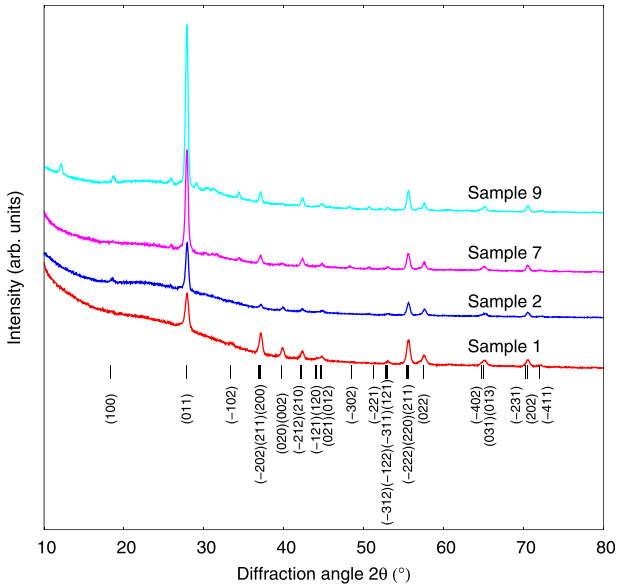

FIG. 6. Glancing incidence X-ray diffractograms taken at room temperature for VO_2-based samples grown under the conditions stated in Table I. The diffraction features are assigned to the shown (*hkl*) planes in monoclinic VO_2.

decreased above τ_c while the infrared reflectance is then increased.

The magnitude of the diffuse components of the transmittance and reflectance is interesting since the analysis to be presented below does not account for them, and also because diffuse optical properties ("haze") may be undesired for practical applications such as in windows. Figure 8 reports $R_d(\lambda)$ and $T_d(\lambda)$ as measured at room temperature for samples 2, 7, and 9 and shows that the diffuse components can be as large as ~12% for $R_d(\lambda)$; the spectra were peaked at a wavelength between 400 and 600 nm. Samples 7 and 9 display well-developed nanofeatures, as seen in Fig. 4, and hence the optical scattering is by no means unexpected. The drop of the diffuse components at the shortest wavelengths is due to absorption in VO_2, and the decline towards longer wavelengths occurs because the ratio between the size of the nanofeatures and the wavelength then gets progressively smaller.

Data on $T(\lambda)$ and $R(\lambda)$ for sample 1 were employed to compute spectral complex dielectric function $\varepsilon_{VO2}(\lambda)$ using commercial software[137] with allowance for a rough surface layer on top of a compact base layer and also including effects of somewhat different reflectance data from the substrate side and the film side of the sample. Figure 9 shows the real and imaginary parts of $\varepsilon_{VO2}(\lambda)$ and compares our results with those earlier reported in the literature.[138–142] Clearly the agreement among the data is satisfactory.

B. Theoretical models

SEM images of the VO_2 deposits, shown in Figs. 3 and 4, were used to formulate structural models which were amenable to calculations of the optical properties for samples 1, 2, 7, and 9 by use of thin film optics.[143] The modeling involves a number of uncertainties, and it does not aim at giving a fully quantitative theoretical representation of the optical properties but rather to explore whether theory and experiment can be brought in qualitative agreement.

Sample 1 is straightforward and can be viewed as a uniform slab of VO_2 characterized by $d = 62.5$ nm. Sample 2 shows signs of porosity, which we represent by $d = f_b d_b$, where f_b denotes a "filling factor" for what we refer to as a "base layer"—i.e., the volume fraction occupied by VO_2—and d_b is the geometrical thickness of this layer. Based on our SEM measurements, we set $d_b = 70$ nm, which yields $f_b = 0.89$. Samples 7 and 9 require more elaborate modeling

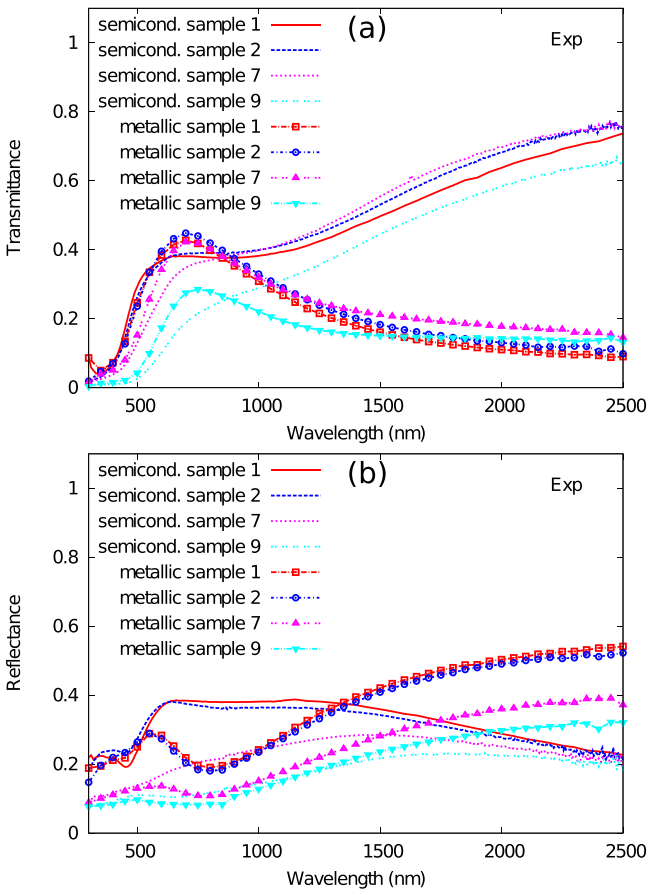

FIG. 7. Experimental spectral total transmittance (a) and reflectance (b) for VO_2-based samples, grown under the conditions given in Table I, in semiconducting and metallic states.

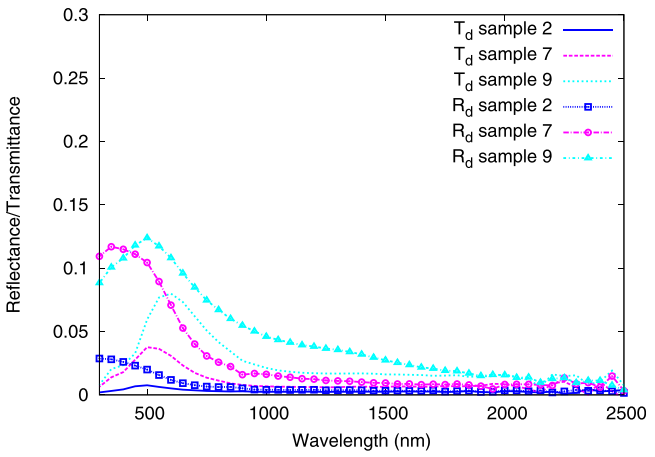

FIG. 8. Spectral diffuse reflectance R_d and transmittance T_d for VO_2-based samples grown under the conditions stated in Table I. Data were taken at room temperature.

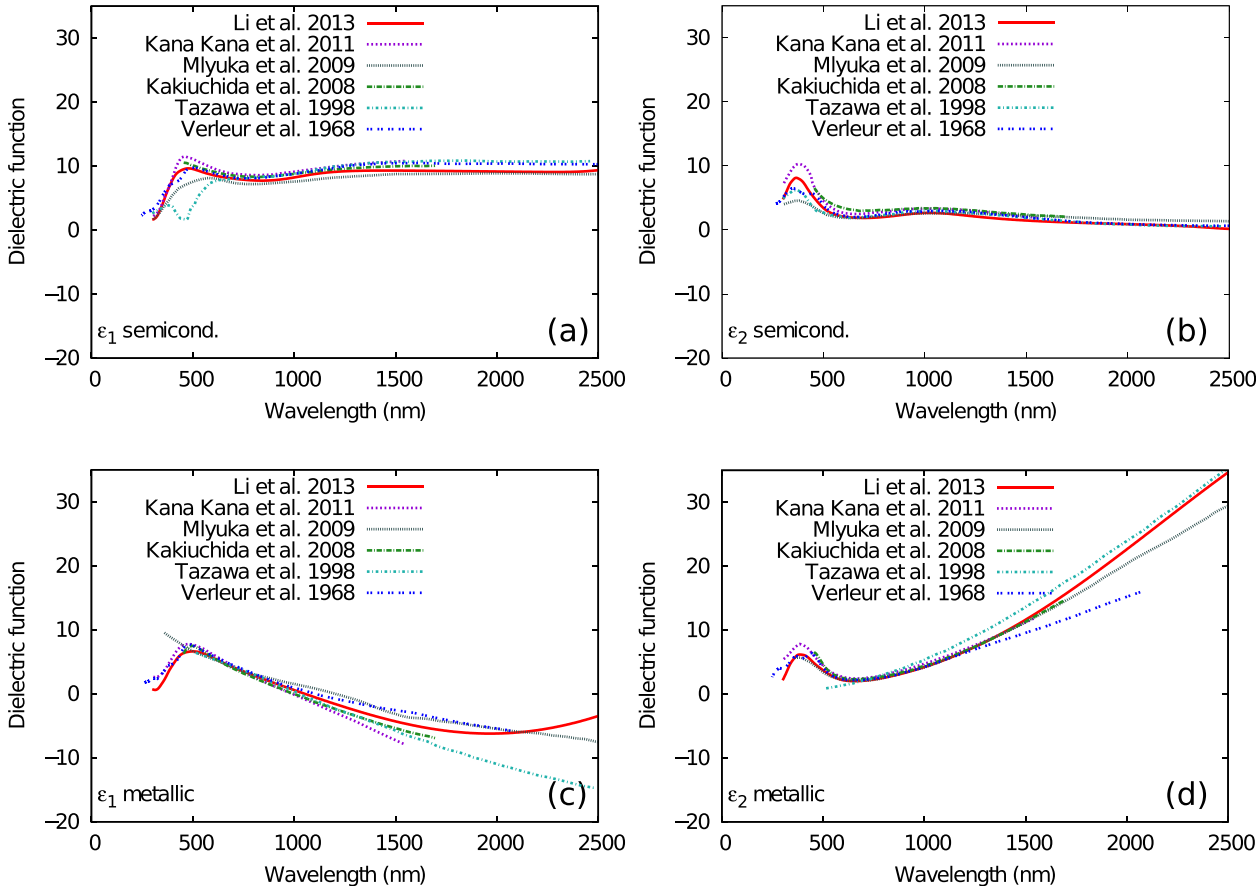

FIG. 9. Complex dielectric function, $\varepsilon \equiv \varepsilon_1 + i\varepsilon_2$, of VO_2 determined from sample 1 grown under the conditions stated in Table I. Upper and lower panels refer to semiconducting and metallic states, respectively. Also shown are data from the literature, specifically from Verleur *et al.* (Ref. 138), Tazawa *et al.* (Ref. 139), Kakiuchida *et al.* (Ref. 140), Mlyuka *et al.* (Ref. 141) and Kana Kana *et al.* (Ref. 142).

and must be described as two-layer structures with a top layer, characterized by a small filling factor f_t and a thickness d_t, overlying a base layer represented by f_b and d_b; these parameters obey the relationship

$$d = f_t d_t + f_b d_b. \tag{1}$$

The shapes and orientations of the nanofeatures are important too. We take the orientations to be random and the shape to be represented by the ratio between the largest and smallest axis of prolate spheroidal ("cigar shaped") units. This ratio is referred to as the "aspect ratio" and is denoted m_t and m_b for the top and base layers, respectively. Close examinations of the SEM images now allow us to assign approximate values to the various parameters, as summarized in Table II.

The optical properties of the top and base layers were accounted for by effective medium theory, which represents their dielectric functions by spatial averages over the properties of the particles ε_p and of their surrounding medium ε_m.[144] Specifically, we used the Bruggeman (BR) formulation,[145] which is appropriate to a random mixture of topologically identical components.[144] This topology seems most appropriate for the relatively dense base layers. Regarding the top layer, one may argue that the sparse VO_2 nanoparticles are embedded in a continuous surrounding medium—which would motivate the use of the Maxwell–Garnett-type effective medium theory[146]—but the values of f_t are so small that the Bruggeman and Maxwell–Garnett theories are predicted to give practically indistinguishable results. Effective medium theory does not account for optical scattering, but the diffuse components of the reflectance and transmittance, shown in Fig. 8, were reassuringly small so as to make our theoretical approach meaningful.

The BR theory gives the effective dielectric function ε^{BR} by

$$\varepsilon^{BR} = \varepsilon_m \frac{1 + \frac{2}{3} f \alpha^{BR}}{1 - \frac{1}{3} f \alpha^{BR}}, \tag{2}$$

$$\alpha^{BR} = \frac{1}{3} \sum_{i=1}^{3} \frac{\varepsilon_p - \varepsilon^{BR}}{\varepsilon^{BR} + L_i(\varepsilon_p - \varepsilon^{BR})}, \tag{3}$$

TABLE II. Parameters for structural models of VO_2-based samples grown under the conditions stated in Table I. d, f, and m denote thickness, filling factor, and aspect ratio, respectively, for top (t) and base (b) layers.

Sample/Model	d_t (nm)	f_t	m_t	d_b (nm)	f_b	m_b
1	…	…	…	62.5	1	…
2	…	…	…	70	0.893	1
7	125	0.05	3	125	0.494	3
9	500	0.01	10	200	0.485	10

where we use the same notation as in earlier papers.[65,67,147,148] Here, the L_is represent triplets of depolarization factors with $L_1 < L_2 = L_3$ and obeying $\Sigma L_i = 1$. For the present case of prolate spheroids, one has[149]

$$L_1 = \frac{1-e^2}{2e^3}\left(\ln\frac{1+e}{1-e} - 2e\right), \tag{4}$$

$$L_2 = L_3 = (1-L_1)/2, \tag{5}$$

$$e = [1-m^{-2}]^{1/2}. \tag{6}$$

As input parameters in Eqs. (2) and (3), we use $\varepsilon_p \equiv \varepsilon_{VO2}$ according to Fig. 9 together with $\varepsilon_m = 1$. Thus, we do not invoke any size dependence in ε_p—as would be required for noble-metal-based particles[147,150]—since the mean free path of the conduction electrons in VO_2 is of the order of inter-atomic distances.[151–153]

C. Comparison of theoretical and experimental data

Figure 10 compares experimental and computed data, specifically the spectral absorptance $A(\lambda) = 1 - T(\lambda) - R(\lambda)$, for four samples. Concerning the experimental results in panel (a), we note that the relatively dense samples 1 and 2 show almost identical absorptance over the whole measured spectral range for both semiconducting and metallic states. This can be compared with $A(\lambda)$ for sample 7, containing nanorods, which shows increased absorption at $300 < \lambda < 1500$ nm for the semiconducting state and a flat upwards shift in the whole spectral range for the metallic state. Sample 9, with nanorods and nanowires, displays an absorptance spectrum similar to that of sample 7 but with significantly increased values over the entire investigated wavelength range, as expected from the difference in mass thickness.

Calculated spectral absorptance is reported in Fig. 10(b) and shows good agreement with the experimental optical data for samples 1 and 2. Furthermore, the calculations exhibit an increasing trend of $A(\lambda)$ as the nanorod content is increased, which is consistent with the experimental data. Especially, the uniform upwards shift at $1000 < \lambda < 2500$ nm, which was apparent in the experimental absorptance for the metallic states of samples 7 and 9, is represented very well by the model. However, the computations display somewhat more pronounced spectral features than the experiments, especially for the semiconducting state. In particular, the absorptance in the ultraviolet and visible ranges for sample 9 clearly exceeds the corresponding calculated result. These effects may be due to the presence of defects, such as an excess of oxygen that is

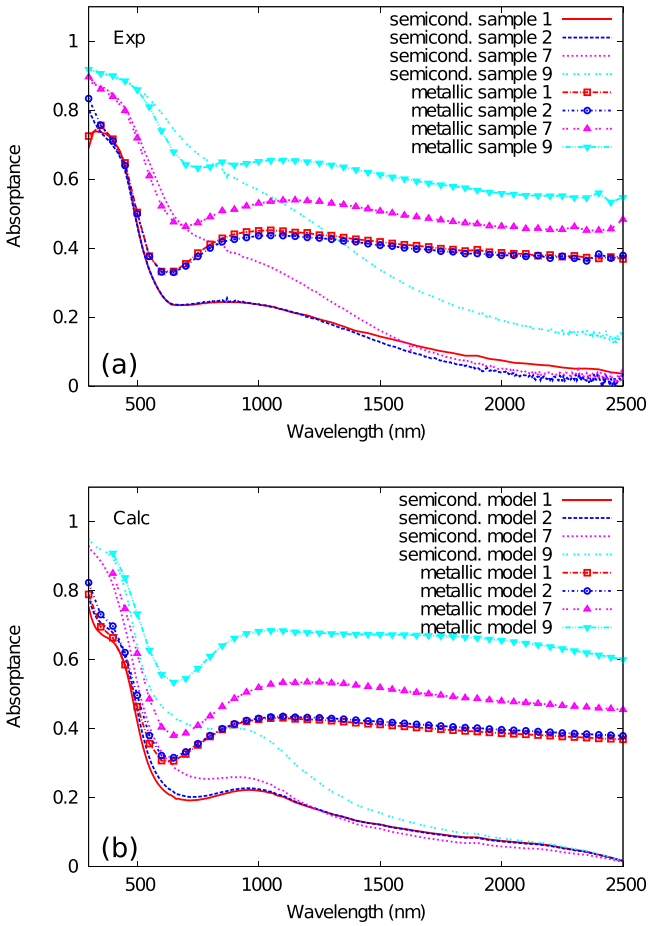

FIG. 10. Spectral absorptance for VO_2-based samples in semiconducting and metallic states. Panel (a) shows experimental data for samples grown under the conditions stated in Table I, and panel (b) reports data obtained from the theoretical model computations and using model parameters given in Table II.

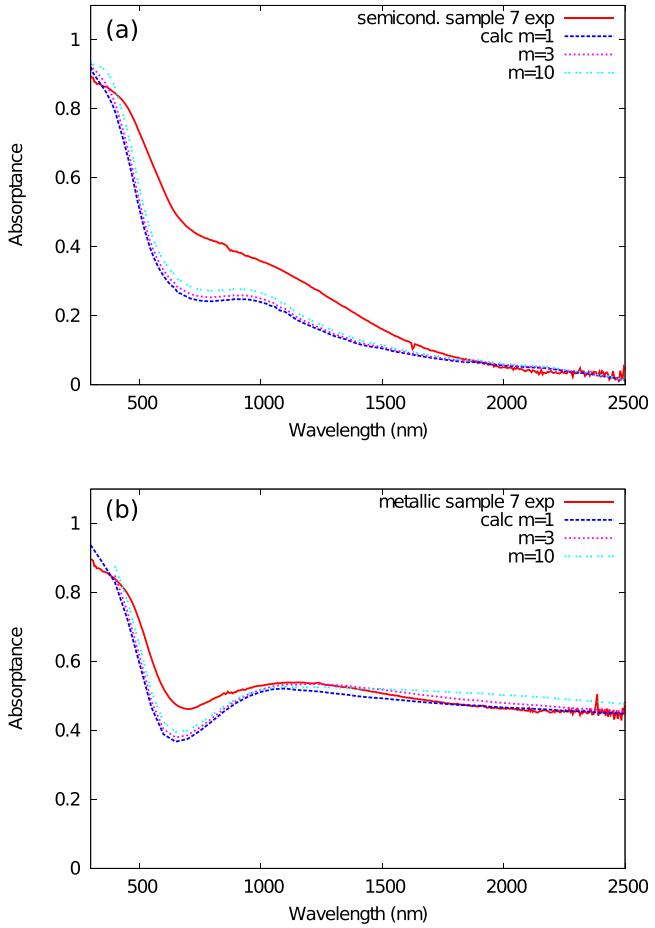

FIG. 11. Spectral absorptance measured for VO_2-based sample 7, grown under the conditions shown in Table I, and obtained from the theoretical model computations and using d_t, d_b, f_t, and f_b given in Table II together with the shown values of $m = m_t = m_b$. Panels (a) and (b) refer to semiconducting and metallic states, respectively. The experimental data were shown also in Fig. 10.

likely to be present at high deposition temperature,[154] or to absorption enhancement by multiple light-scattering.

It is worth noting that effective medium theory could no longer fully describe the optical properties in the short wavelength range for samples 7 and 9, which is understandable since the diffuse transmittance and reflectance were not negligible, as apparent from Fig. 8.

The theoretical models contain numerous parameters, and it is essential to ascertain that the results in Fig. 10 are neither fortuitous nor critically sensitive to the choice of parameter values. To this end we selected sample 7 for in-depth analysis and carried out calculations not only for $m_t = m_b = 3$, as before, but also for aspects ratios of 1 (spheres) and 10. Figure 11 demonstrates that the role of the nanorod shape is minor. We also analyzed sample 7 by calculations regarding the effect of (i) having only the base layer on the glass substrate, (ii) having nothing but the top layer, and (iii) assuming that all of the VO_2 is accounted for by the base layer. Figure 12 shows that the absorption of the top layer alone is not negligible, but when this layer is added to the base layer there is a reduction of the light available for absorption in the base layer, the net effect being that the total absorption in the metallic state within the double-layer model yields merely a minor increase, on the scale of ~0.04 for the near-infrared absorption, compared with the case of having the base layer encompass all of the VO_2. In the semiconducting state, the contribution of the top layer is even smaller. The main conclusion from the data presented in Figs. 11 and 12 is that the results inferred from Fig. 10 are reliable and not dependent on the details of the theoretical models.

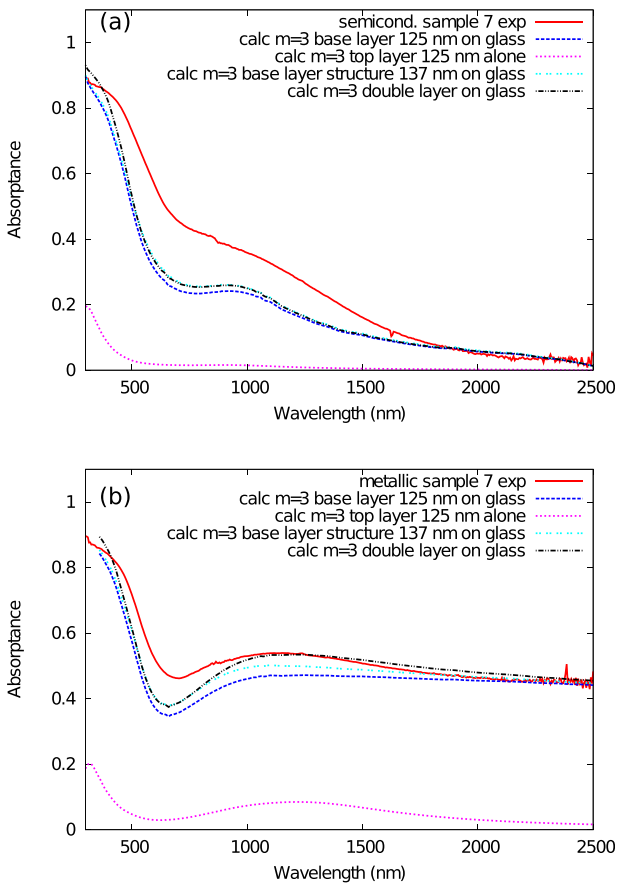

FIG. 12. Spectral absorptance measured for VO_2-based sample 7, grown under the conditions shown in Table I, and obtained from the theoretical model computations and using the model parameters given in Table II (marked as "double layer on glass"). Also reported are computational results for a 125-nm-thick base layer on glass, a 125-nm-thick top layer alone, a 137-nm-thick film (with the total amount of VO_2 encompassed by the double layer model) having the same structure as the base layer. Panels (a) and (b) refer to semiconducting and metallic states, respectively. The experimental data were shown also in Fig. 10.

V. CONCLUSION AND REMARKS

This work has demonstrated that reactive dc magnetron sputtering is a viable technique for preparing deposits of VO_2 nanorods and nanowires. Their formation was found to be strongly influenced by several deposition conditions: (i) the substrate temperature should be relatively high and 550 °C was superior to 450 °C, (ii) the deposit thickness should be large enough and our best data were obtained for the thickest layer with a mass thickness of ~100 nm, (iii) a thin layer of gold seeds promoted nanorod and nanowire formation, (iv) nanostructuring of the substrate facilitated nanowire formation, and (v) the "gas geometry"—i.e., the provisions for reactive gas inlet in the sputter chamber—was of large significance.

The growth conditions leading to VO_2 nanorods and nanowires are unclear but may be related to the mechanisms underlying high-temperature glancing angle deposition (known as "HT-GLAD").[155–159] For the case of metal nanowires, the substrate temperature should be higher than about one third of the metal's melting point and the deposition angle typically should exceed 80° with regard to the substrate normal. For the VO_2 nanowires in the present study, we expect that the relative magnitude of the fluxes of vanadium atoms and oxygen molecules plays a decisive role. These aspects, and their interpretation in terms of HT-GLAD, will be treated in a forthcoming publication. The beneficial effect of gold seeds may be related to the well-known gold-catalyzed vapor–liquid–solid growth mode of semiconductor nanowires.[160]

The spectral absorptance of our deposits could be reconciled with an effective medium treatment based on the Bruggeman theory and using empirical data on the complex dielectric function of VO_2.

ACKNOWLEDGMENTS

This work was financially supported by the Japan Society for the Promotion of Science (JSPS) through JSPS KAKENHI Grant No. 24-2362 and the JSPS Institutional Program for Young Researcher Overseas Visits. Further financial support was received from the Swedish Research Council. We acknowledge assistance with RBS measurements from Daniel Primetzhofer and the staff of the Tandem Accelerator Laboratory at Uppsala University and assistance with SEM measurements from Sadamu Kinoshita at Kyoto University. S.-Y.L. is grateful to Bozhidar Stefanov, Malin Johansson, Wei Xia, Ruitao Wen, and Anil Kumar Puri for discussions concerning XRD.

[1]F. J. Morin, Phys. Rev. Lett. **3**, 34 (1959).
[2]M. M. Qazilbash, A. Tripathi, A. A. Schafgans, B.-J. Kim, H.-T. Kim, Z. Cai, M. V. Holt, J. M. Maser, F. Keilmann, O. G. Shpyrko, and D. N. Basov, Phys. Rev. B **83**, 165108 (2011).
[3]A. S. Belozerov, M. A. Korotin, V. I. Anisimov, and A. I. Poteryaev, Phys. Rev. B **85**, 045109 (2012).

[4]J. S. Lee, K. Shibuya, M. Kawasaki, and Y. Tokura, Phys. Rev. B **85**, 155110 (2012).
[5]M. Liu, H. Y. Hwang, H. Tao, A. C. Strikwerda, K. Fan, G. R. Keiser, A. J. Sternbach, K. G. West, S. Kittiwatanakul, J. Lu, S. A. Wolf, F. G. Omenetto, X. Zhang, K. A. Nelson, and R. D. Averitt, Nature **487**, 345 (2012).
[6]A. Pergament and G. Stefanovich, Phase Transitions **85**, 185 (2012).
[7]C. Si, W. Xu, H. Wang, J. Zhou, A. Ablat, L. Zhang, J. Cheng, Z. Pan, L. Fan, C. Zou, and Z. Wu, Phys. Chem. Chem. Phys. **14**, 15021 (2012).
[8]Z. Tao, T.-R. T. Han, S. D. Mahanti, P. M. Duxbury, F. Yuan, and C.-Y. Ruan, Phys. Rev. Lett. **109**, 166406 (2012).
[9]X. Zhong, P. LeClair, S. K. Sarker, and A. Gupta, Phys. Rev. B **86**, 094114 (2012).
[10]J. B. Goodenough, J. Solid State Chem. **3**, 490 (1971).
[11]S.-Y. Li, G. A. Niklasson, and C. G. Granqvist, Thin Solid Films **520**, 3823 (2012).
[12]J. Wei, H. Ji, W. Guo, A. H. Nevidomskyy, and D. Natelson, Nat. Nanotechnol. **7**, 357 (2012).
[13]Y. Cui and S. Ramanathan, J. Vac. Sci. Technol. A **29**, 041502 (2011).
[14]N. R. Mlyuka, G. A. Niklasson, and C. G. Granqvist, Appl. Phys. Lett. **95**, 171909 (2009).
[15]S. Hu, S.-Y. Li, R. Ahuya, C. G. Granqvist, K. Hermansson, G. A. Niklasson, and R. H. Scheicher, Appl. Phys. Lett. **101**, 201902 (2012).
[16]K. A. Khan and C. G. Granqvist, Appl. Phys. Lett. **55**, 4 (1989).
[17]V. N. Andreev and V. A. Klimov, Fiz. Tverd. Tela **53**, 538 (2012) [Phys. Solid State **53**, 577 (2011)].
[18]J. M. Atkin, S. Beerweger, E. K. Chavez, M. B. Raschke, J. Cao, W. Fan, and J. Wu, Phys. Rev. B **85**, 020101 (2012).
[19]J. Laverock, L. F. J. Piper, A. R. H. Preston, B. Chen, J. McNulty, K. E. Smith, S. Kittiwatanakul, J. W. Lu, S. A. Wolf, P.-A. Glans, and J.-H. Guo, Phys. Rev. B **85**, 081104 (2012).
[20]G. J. Kovács, D. Bürger, I. Skorupa, H. Reuther, R. Heller, and H. Schmidt, J. Appl. Phys. **109**, 063708 (2011).
[21]H. Koo, S. Yoon, O.-J. Kwon, K.-E. Ko, D. Shin, S.-H. Bae, S.-H. Chang, and C. Park, J. Mater. Sci. **47**, 6397 (2012).
[22]S. D. Ha, G. H. Aydogdu, B. Viswanath, and S. Ramanathan, J. Appl. Phys. **110**, 026110 (2011).
[23]Y.-G. Jeong, H. Bernien, J.-S. Kyoung, H.-R. Park, H.-S. Kim, J.-W. Choi, B.-J. Kim, H.-T. Kim, K. J. Ahn, and D.-S. Kim, Opt. Express **19**, 21211 (2011).
[24]Z. Yang, S. Hart, C. Ko, A. Yacoby, and S. Ramanathan, J. Appl. Phys. **110**, 033725 (2011).
[25]T. Driscoll, J. Quinn, M. Di Ventra, D. N. Basov, G. Seo, Y.-W. Lee, H.-T. Kim, and D. R. Smith, Phys. Rev. B **86**, 094203 (2012).
[26]B. A. Kruger, A. Joushaghani, and J. K. S. Poon, Opt. Express **20**, 23598 (2012).
[27]Y. Liu, E. Uchaker, N. Zhou, J. Li, Q. Zhang, and G. Cao, J. Mater. Chem. **22**, 24439 (2012).
[28]M. Nakano, K. Shibuya, D. Okuyama, T. Hatano, S. Ono, M. Kawasaki, Y. Iwasa, and Y. Tokura, Nature **487**, 459 (2012).
[29]A. B. Pevtsov, A. V. Medvedev, D. A. Kurdyukov, N. D. Il'inskaya, V. G. Golubev, and V. G. Karpov, Phys. Rev. B **85**, 024110 (2012).
[30]Z. Yang, Y. Zhou, and S. Ramanathan, J. Appl. Phys. **111**, 014506 (2012).
[31]Y. Zhao, J. Hao, C. Chen, and Z. Fan, J. Phys.: Condens. Matter **24**, 035601 (2012).
[32]H. Dachraoui, N. Müller, G. Obermeier, C. Oberer, S. Horn, and U. Heinzmann, J. Phys.: Condens. Matter **23**, 435402 (2011).
[33]D. W. Ferrara, E. R. MacQuarrie, J. Nag, A. B. Kaye, and R. F. Haglund, Jr., Appl. Phys. Lett. **98**, 241112 (2011).
[34]A. Pashkin, C. Kübler, H. Ehrke, R. Lopez, A. Halabica, R. F. Haglund, Jr., R. Huber, and A. Leitenstorfer, Phys. Rev. B **83**, 195120 (2011).
[35]A. L. Semenov, Fiz. Tverd. Tela **53**, 361 (2011) [Phys. Solid State **53**, 386 (2011)].
[36]N. Dávila, R. Cabrera, and N. Sepúlveda, IEEE Photonics Technol. Lett. **24**, 1830 (2012).
[37]P. A. Do, A. Hendaoui, E. Mortazy, M. Chaker, and A. Haché, Opt. Commun. **288**, 23 (2013).
[38]G. Seo, B.-J. Kim, Y. W. Lee, and H.-T. Kim, Appl. Phys. Lett. **100**, 011908 (2012).
[39]A. Gupta, R. Singhal, J. Narayan, and D. K. Avasthi, J. Mater. Res. **26**, 2901 (2011).
[40]H. Hofsäss, P. Ehrhardt, H.-G. Gehrke, M. Brötzmann, U. Vetter, K. Zhang, J. Krauser, C. Trautmann, C. Ko, and S. Ramanathan, AIP Adv. **1**, 032168 (2011).
[41]J. W. Byon, M.-B. Kim, M. H. Kim, S. Y. Kim, S. H. Lee, B. C. Lee, and J. M. Baik, J. Phys. Chem. C **116**, 226 (2012).
[42]S. M. Babulanam, T. S. Eriksson, G. A. Niklasson, and C. G. Granqvist, Sol. Energy Mater. **16**, 347 (1987).
[43]C. G. Granqvist, Sol. Energy Mater. Sol. Cells **91**, 1529 (2007).
[44]M. Saeli, C. Piccirillo, I. P. Parkin, R. Binions, and I. Ridley, Energy Build. **42**, 1666 (2010).
[45]M. Saeli, C. Piccirillo, I. P. Parkin, I. Ridley, and R. Binions, Sol. Energy Mater. Sol. Cells **94**, 141 (2010).
[46]G. B. Smith and C. G. Granqvist, *Green Nanotechnology: Solutions for Sustainability and Energy in the Built Environment* (CRC Press, Boca Raton, FL, 2010).
[47]Z. Chen, Y. Gao, L. Kang, J. Du, Z. Zhang, H. Luo, H. Miao, and G. Tan, Sol. Energy Mater. Sol. Cells **95**, 2677 (2011).
[48]Z. Zhang, Y. Gao, H. Luo, L. Kang, Z. Chen, J. Du, M. Kanehira, Y. Zhang, and Z. L. Wang, Energy Environ. Sci. **4**, 4290 (2011).
[49]Y. Gao, H. Luo, Z. Zhang, L. Kang, Z. Chen, J. Du, M. Kanehira, and C. Cao, Nano Energy **1**, 221 (2012).
[50]Y. Gao, S. Wang, L. Kang, Z. Chen, J. Du, X. Liu, H. Luo, and M. Kanehira, Energy Environ. Sci. **5**, 8234 (2012).
[51]M. Benkahoul, M. Chaker, J. Margot, E. Haddad, R. Kruzelecky, B. Wong, W. Jamroz, and P. Poinas, Sol. Energy Mater. Sol. Cells **95**, 3504 (2011).
[52]G. Seo, B.-J. Kim, Y. W. Lee, S. Choi, J.-H. Shin, and H.-T. Kim, Thin Solid Films **519**, 3383 (2011).
[53]M. Soltani, M. Chaker, and J. Margot, Sci. Technol. Adv. Mater. **12**, 045002 (2011).
[54]S. Sengupta, K. Wang, K. Liu, A. K. Bhat, S. Dhara, J. Wu, and M. M. Deshmukh, Appl. Phys. Lett. **99**, 062114 (2011).
[55]Y. Zhou and S. Ramanathan, J. Appl. Phys. **111**, 084508 (2012).
[56]A. Tselev, J. D. Budai, E. Strelcov, J. Z. Tischler, A. Kolmakov, and S. V. Kalinin, Nano Lett. **11**, 3065 (2011).
[57]A. Rúa, R. Cabrera, H. Coy, E. Merced, N. Sepúlveda, and F. E. Fernández, J. Appl. Phys. **111**, 104502 (2012).
[58]L. Pellegrino, N. Manca, T. Kanki, H. Tanaka, M. Biasotti, E. Bellingeri, A. S. Siri, and D. Marré, Adv. Mater. **24**, 2929 (2012).
[59]S. B. Choi, J. S. Kyoung, H. S. Kim, H. R. Park, D. J. Park, B.-J. Kim, Y. H. Ahn, F. Rotermund, H.-T. Kim, K. J. Ahn, and D. S. Kim, Appl. Phys. Lett. **98**, 071105 (2011).
[60]M. J. Coppinger, N. A. Sustersic, J. Kolodzey, and T. H. Allik, Opt. Eng. **50**, 053206 (2011).
[61]L. N. Son, T. Tachiki, and T. Uchida, Jpn. J. Appl. Phys., Part 1 **50**, 025803 (2011).
[62]H. Takami, K. Kawatani, T. Kamki, and H. Tanaka, Jpn. J. Appl. Phys., Part 1 **50**, 055804 (2011).
[63]B. Wang, J. Lai, E. Zhao, H. Hu, Q. Liu, and S. Chen, Opt. Eng. **51**, 074003 (2012).
[64]H. Yin, K. Yu, Z. Zhang, M. Zeng, L. Lou, and Z. Zhu, Electroanalysis **23**, 1752 (2011).
[65]S.-Y. Li, G. A. Niklasson, and C. G. Granqvist, J. Appl. Phys. **108**, 063525 (2010).
[66]S.-Y. Li, G. A. Niklasson, and C. G. Granqvist, J. Appl. Phys. **109**, 113515 (2011).
[67]S.-Y. Li, G. A. Niklasson, and C. G. Granqvist, Appl. Phys. Lett. **99**, 131907 (2011).
[68]S. Ji, F. Zhang, and P. Jin, J. Solid State Chem. **184**, 2285 (2011).
[69]S. Ji, F. Zhang, and P. Jin, Sol. Energy Mater. Sol. Cells **95**, 3520 (2011).
[70]S. Ji, F. Zhang, and P. Jin, Mater. Lett. **65**, 708 (2011).
[71]W. Jiang, J. Ni, K. Yu, and Z. Zhu, Appl. Surf. Sci. **257**, 3253 (2011).
[72]F. Y. Kong, M. Li, S. S. Pan, Y. X. Zhang, and G. H. Li, Mater. Res. Bull. **46**, 2100 (2011).
[73]H. Li, P. He, Y. Wang, E. Hosono, and H. Zhou, J. Mater. Chem. **21**, 10999 (2011).
[74]M. Li, F. Kong, Y. Zhang, and G. Li, Cryst. Eng. Comm. **13**, 2204 (2011).
[75]M. Li, F. Kong, L. Li, Y. Zhang, L. Chen, W. Yan, and G. Li, Dalton Trans. **40**, 10961 (2011).
[76]A. Llordes, A. T. Hammack, R. Buonsanti, R. Tangirala, S. Aloni, B. A. Helms, and D. J. Milliron, J. Mater. Chem. **21**, 11631 (2011).
[77]Z. Lu, C. Li, and Y. Yin, J. Mater. Chem. **21**, 14776 (2011).
[78]H. Miyazaki, K. Yoshida, S. Sasaki, N. Sakamoto, N. Wakiya, H. Suzuki, and T. Ota, J. Ceram. Soc. Jpn. **119**, 522 (2011).
[79]J. Ni, W. Jiang, K. Yu, Y. Gao, and Z. Zhu, Electrochim. Acta **56**, 2122 (2011).

[80]J. Ni, W. Jiang, K. Yu, F. Sun, and Z. Zhu, Cryst. Res. Technol. **46**, 507 (2011).
[81]S. Ni, H. Zeng, and X. Yang, J. Nanomater. **2011**, 961389 (2011).
[82]Y. Sun, S. Jiang, W. Bi, R. Long, X. Tan, C. Wu, S. Wei, and Y. Xie, Nanoscale **3**, 4394 (2011).
[83]L. Whittaker, J. M. Velazquez, and S. Banerjee, Cryst. Eng. Comm. **13**, 5328 (2011).
[84]L. Whittaker, T.-L. Wu, C. J. Patridge, S. Sambandamurthy, and S. Banerjee, J. Mater. Chem. **21**, 5580 (2011).
[85]C. Wu, X. Zhang, J. Dai, J. Yang, Z. Wu, S. Wie, and Y. Xie, J. Mater. Chem. **21**, 4509 (2011).
[86]T.-L. Wu, L. Whittaker, S. Banerjee, and G. Sambandamurthy, Phys. Rev. B **83**, 073101 (2011).
[87]H. Yin, M. Luo, K. Yu, Y. Gao, R. Huang, Z. Zhang, M. Zeng, C. Cao, and Z. Zhu, ACS Appl. Mater. Interfaces **3**, 2057 (2011).
[88]H. Yin, J. Ni, W. Jiang, Z. Zhang, and K. Yu, Physica E **43**, 1720 (2011).
[89]H. Yin, K. Yu, Z. Zhang, and Z. Zhu, Appl. Surf. Sci. **257**, 8840 (2011).
[90]S. Zhang, B. Shang, J. Yang, W. Yan, S. Wei, and Y. Xie, Phys. Chem. Chem. Phys. **13**, 15873 (2011).
[91]Y. Zhang, M. Fan, F. Niu, Y. Zhong, C. Huang, X. Liu, B. Wang, and H. Li, Micro Nano Lett. **6**, 888 (2011).
[92]Y. Zhang, C. Chen, J. Zhang, L. Hu, W. Wu, Y. Zhong, Y. Cao, and X. Liu, Curr. Appl. Phys. **13**, 47 (2013).
[93]Y. Zhang, M. Fan, W. Wu, L. Hu, J. Zhang, Y. Mao, C. Huang, and X. Liu, Mater. Lett. **71**, 127 (2012).
[94]Y. Zhang, Y. Huang, J. Zhang, W. Wu, F. Niu, Y. Zhong, X. Liu, X. Liu, and C. Huang, Mater. Res. Bull. **47**, 1978 (2012).
[95]Y. Zhang, M. Fan, X. Liu, G. Xie, H. Li, and C. Huang, Solid State Commun. **152**, 253 (2012).
[96]Y. Zhang, M. Fan, F. Niu, W. Wu, C. Huang, X. Liu, H. Li, and X. Liu, Curr. Appl. Phys. **12**, 875 (2012).
[97]Y. Zhang, M. Fan, M. Zhou, C. Huang, C. Chen, Y. Cao, G. Xie, H. Li, and X. Liu, Bull. Mater. Sci. **35**, 369 (2012).
[98]Y. Zhang, F. Zhang, L. Yu, M. Fan, Y. Zhong, X. Liu, Y. Mao, and C. Huang, Colloids Surf., A **396**, 144 (2012).
[99]Y. Zhang, J. Zhang, Y. Zhong, L. Yu, Y. Deng, C. Huang, and X. Liu, Appl. Surf. Sci. **263**, 124 (2012).
[100]Q. Zhao, L. Jiao, W. Peng, H. Gao, J. Yang, Q. Wang, H. Du, L. Li, Z. Qi, Y. Si, Y. Wang, and H. Yuan, J. Power Sources **199**, 350 (2012).
[101]L. Chen, C. Huang, G. Xu, L. Miao, J. Shi, J. Zhou, and X. Xiao, J. Nanomater. **2012**, 491051.
[102]Y. Gao, C. Cao, L. Dai, H. Luo, M. Kanehira, Y. Ding, and Z. L. Wang, Energy Environ. Sci. **5**, 8708 (2012).
[103]Y. Gao, S. Wang, H. Luo, L. Dai, C. Cao, Y. Liu, Z. Chen, and M. Kanehira, Energy Environ. Sci. **5**, 6104 (2012).
[104]S. Milošević, I. Stojković, S. Kurko, J. Grbović Novaković, and N. Cvjetićanin, Ceram. Int. **38**, 2313 (2012).
[105]C. Nethravathi, B. Viswanath, J. Michael, and M. Rajamath, Carbon **50**, 4839 (2012).
[106]C. J. Partridge, L. Whittaker, B. Ravel, and S. Banerjee, J. Phys. Chem. C **116**, 3728 (2012).
[107]X. Rui, D. Sim, C. Xu, W. Liu, H. Tan, K. Wong, H. H. Hng, T. M. Lim, and Q. Yan, RSC Adv. **2**, 1174 (2012).
[108]L. Soltane, F. Sediri, and N. Gharbi, Mater. Res. Bull. **47**, 1615 (2012).
[109]H. Guo, K. Chen, Y. Oh, K. Wang, C. Dejoie, S. A. Syed Asif, O. L. Warren, Z. W. Shan, J. Wu, and A. M. Minor, Nano Lett. **11**, 3207 (2011).
[110]S. Löffler, E. Auer, M. Weil, A. Lugstein, and E. Bertagnolli, Appl. Phys. A **102**, 201 (2011).
[111]E. Strelcov, A. V. Davydov, U. Lanke, C. Watts, and A. Kolmakov, ACS Nano **5**, 3373 (2011).
[112]J. M. Wu and L. B. Liou, J. Mater. Chem. **21**, 5499 (2011).
[113]R. Xie, C. T. Bui, B. Varghese, Q. Zhang, C. H. Sow, B. Li, and J. T. L. Thong, Adv. Funct. Mater. **21**, 1602 (2011).
[114]S. Zhang, I. S. Kim, and L. J. Lauhon, Nano Lett. **11**, 1443 (2011).
[115]J. I. Sohn, H. J. Joo, K. S. Kim, H. W. Yang, A.-R. Jang, D. Ahn, H. H. Lee, S. Cha, D. J. Kang, J. M. Kim, and M. E. Welland, Nanotechnology **23**, 205707 (2012).
[116]Y. Yang, K. Lee, M. Zobel, M. Maćović, T. Unruh, E. Spiecker, and P. Schmulki, Adv. Mater. **24**, 1571 (2012).
[117]L. Kang, Y. Gao, H. Luo, Z. Chen, J. Du, and Z. Zhang, Appl. Mater. Interfaces **3**, 135 (2011).
[118]L. Kang, Y. Gao, H. Luo, J. Wang, B. Zhu, Z. Zhang, J. Du, M. Kanehira, and Y. Zhang, Sol. Energy Mater. Sol. Cells **95**, 3189 (2011).
[119]D. A. Kurdyukov, S. A. Grudinkin, A. V. Nashchekin, A. N. Smirnov, E. Yu. Trofimova, M. A. Yagovkina, A. B. Pevtsov, and V. G. Golubev, Fiz. Tverd. Tela **53**, 400 (2011) [Phys. Solid State **53**, 428 (2011)].
[120]C. Cheng, K. Liu, B. Xiang, J. Suh, and J. Wu, Appl. Phys. Lett. **100**, 103111 (2012).
[121]H. J. Gläser, *Large Area Glass Coating* (von Ardenne Anlagentechnik GmbH, Dresden, Germany, 2000).
[122]C. G. Granqvist, Sol. Energy Mater. Sol. Cells **99**, 166 (2012).
[123]K. Namura, M. Suzuki, K. Nakajima, and K. Kimura, Opt. Lett. **36**, 3533 (2011).
[124]S. Norrman, T. Andersson, C. G. Granqvist, and O. Hunderi, Phys. Rev. B **18**, 674 (1978).
[125]G. B. Smith, G. A. Niklasson, J. S. E. M. Svensson, and C. G. Granqvist, J. Appl. Phys. **59**, 571 (1986).
[126]P. C. Lansåker, J. Backholm, G. A. Niklasson, and C. G. Granqvist, Thin Solid Films **518**, 1225 (2009).
[127]P. C. Lansåker, P. Petersson, G. A. Niklasson, and C. G. Granqvist, (to be published).
[128]M. Mayer, AIP Conf. Proc. **475**, 541 (1999).
[129]Joint Center for Powder Diffraction Spectra, JCPDS Card No. 43–1051.
[130]H. M. Rietveld, J. Appl. Crystallogr. **2**, 65 (1969).
[131]G. Nolze and W. Kraus, *PowderCell 2.3 Program* (Federal Institute for Materials Research and Testing, Berlin, Germany, 2000).
[132]W. A. Dollase, J. Appl. Crystallogr. **19**, 267 (1986).
[133]Joint Center for Powder Diffraction Spectra, JCPDS Card No. 89–0612.
[134]Joint Center for Powder Diffraction Spectra, JCPDS Card No. 45–1074.
[135]Joint Center for Powder Diffraction Spectra, JCPDS Card No. 35–0361.
[136]D. Barrios, R. Vergaz, J. M. Sanchez-Pena, C. G. Granqvist, and G. A. Niklasson, Sol. Energy Mater. Sol. Cells **111**, 115 (2013).
[137]M. Theiss, *Hard and Software for Optical Spectroscopy* (Dr.-Bernhard-Klein-Str. 110, D-52078 Aachen, Germany, 2002), see http://www.mtheiss.com.
[138]H. W. Verleur, A. S. Barker, Jr., and C. N. Berglund, Phys. Rev. **172**, 788 (1968).
[139]M. Tazawa, P. Jin, and S. Tanemura, Appl. Opt. **37**, 1858 (1998).
[140]H. Kakiuchida, P. Jin, and M. Tazawa, Sol. Energy Mater. Sol. Cells **92**, 1279 (2008).
[141]N. R. Mlyuka, G. A. Niklasson, and C. G. Granqvist, Phys. Status Solidi A **206**, 2155 (2009).
[142]J. B. Kana Kana, J. M. Ndjaka, G. Vignaud, A. Gibaud, and M. Maaza, Opt. Commun. **284**, 807 (2011).
[143]M. Born and E. Wolf, *Principles of Optics*, 7th ed. (Cambridge University Press, Cambridge, UK, 1999).
[144]G. A. Niklasson, C. G. Granqvist, and O. Hunderi, Appl. Opt. **20**, 26 (1981).
[145]D. A. G. Bruggeman, Ann. Phys. (Leipz.) **416**, 636 (1935).
[146]J. C. Maxwell-Garnett, Philos. Trans. R. Soc. London, Ser. A **203**, 385 (1904); **205**, 237 (1906).
[147]C. G. Granqvist and O. Hunderi, Phys. Rev. B **16**, 3513 (1977).
[148]C. G. Granqvist and O. Hunderi, Phys. Rev. B **18**, 2897 (1978).
[149]E. M. Lifshitz, L. D. Landau, and L. P. Pitaevskii, *Electrodynamics of Continuous Media*, 2nd ed. (Butterworth–Heinemann, Burlington, MA, 1984).
[150]U. Kreibig and M. Vollmer, *Optical Properties of Metal Clusters* (Springer, Berlin, Germany, 1995).
[151]P. B. Allen, R. M. Wentzcovitch, W. W. Schulz, and P. C. Canfield, Phys. Rev. B **48**, 4359 (1993).
[152]K. Okazaki, S. Sugai, Y. Muraoka, and Z. Hiroi, Phys. Rev. B **73**, 165116 (2006).
[153]A. Gentle, A. I. Maaroof, and G. B. Smith, Nanotechnology **18**, 025202 (2007).
[154]C. Chen and Z. Fan, Appl. Phys. Lett. **95**, 262106 (2009).
[155]M. Suzuki, K. Nagai, S. Kinoshita, K. Nakajima, K. Kimura, T. Okano, and K. Sasakawa, Appl. Phys. Lett. **89**, 133103 (2006).
[156]M. Suzuki, K. Hamachi, K. Nagai, R. Kita, K. Nakajima, and K. Kimura, ECS Trans. **33**(9), 41 (2010).
[157]M. Suzuki, R. Kita, H. Hara, K. Hamachi, K. Nagai, K. Nakajima, and K. Kimura, J. Electrochem. Soc. **157**, K34 (2010).
[158]M. Suzuki, K. Hamachi, H. Hara, K. Nakajima, K. Kimura, C.-W. Hsu, and L.-J. Chou, Appl. Phys. Lett. **99**, 223107 (2011).
[159]K. Hamachi, M. Suzuki, K. Nakajima, and K. Kimura, MRS Proc. **1059**, 1059-KK04-09 (2007).
[160]R. S. Wagner and W. C. Ellis, Appl. Phys. Lett. **4**, 89 (1964).